Available online at www.sciencedirect.com
SCIENCE DIRECT®
Journal of Contaminant Hydrology 77 (2005) 271–297
JOURNAL OF Contaminant Hydrology
www.elsevier.com/locate/jconhyd

Effects of skin and hydraulic fractures on SVE wells

Graham C. Bradner[a,1], Lawrence C. Murdoch[b,*]

[a]*Geosyntec Consultants, 475 14th Street, Ste. 450, Oakland, CA 94612, United States*
[b]*Clemson University, Department of Geosciences, 340 Brackett Hall, Clemson, SC 29634, United States*

Received 19 December 2003; received in revised form 19 January 2005; accepted 9 February 2005

Abstract

Soil vapor extraction (SVE) systems are intended to cause substantial volumes of air to flow through the subsurface with the purpose of removing volatile contaminants. The effectiveness of SVE can be influenced by any effect that changes the specific gas capacity (discharge as a function of vacuum) of a well. Skins of low permeability material enveloping a well bore are widely recognized to affect the performance of wells used to recover water, natural gas, or petroleum, and skin can also significantly diminish the performance of an SVE well. Skins a few mm thick consisting of material whose gas phase permeability is 0.01 of the formation can reduce the specific gas capacity of an SVE well by factors of 2 to 10 or more. Hydraulic fractures created in the vicinities of shallow wells commonly resemble sand-filled layers shaped like flat-lying disks or gently dipping saucers. The contrast between the gas-phase permeability of the sand in the fracture and that of the formation is particularly important, with significant effects requiring the ratio to be greater than approximately 50. Shallow hydraulic fractures filled with several tenths of m^3 of sand in formations that are several orders of magnitude less permeable than that of the enveloping formation should increase specific gas capacity by factors of 10 or more. Field tests of the effects of hydraulic fractures on the performance of SVE were conducted by creating four wells intersecting fractures and a suite of control wells created using conventional methods in silty saprolite. Specific gas capacities ranged over more than an order of magnitude for 10 wells completed within a small area (2 m^2) and at the same depth. Specific capacities correlate to the drilling method that was used to create the bore for the well: lowest values occurred in wells drilled with a machine auger, slightly better results were obtained using a Shelby tube, and the best results were obtained from conventional wells bored with a hand auger. Skin factors determined for wells created with a machine auger could be explained by a

* Corresponding author. Tel.: +1 864 656 2597; fax: +1 864 656 1041.
E-mail addresses: gbradner@geosyntec.com (G.C. Bradner), lmurdoch@clemson.edu (L.C. Murdoch).
[1] Tel.: +1 925 943 3034; fax: +1 925 943 2366.

0169-7722/$ - see front matter
doi:10.1016/j.jconhyd.2005.02.001

layer 1 cm thick that has 0.007 times the permeability of the enveloping material, which could readily have been created during the drilling procedure. Specific capacities of wells intersecting hydraulic fractures were 5 to 100 times more than those of conventional wells. The large difference in performance appears to be due in part to the beneficial effects of the fracture, and in part to the detrimental effects of well skin.

Keywords: Soil vapor extraction; Hydraulic fractures; Well testing; Well skin

1. Introduction

Soil vapor extraction (SVE) is perhaps the most successful method of remediating the unsaturated zone, with thousands of contaminated sites benefiting from this technology (Gierke, 2000). The overall performance of SVE is limited by the magnitude and distribution of flow through the subsurface and the rate of mass transfer between contaminants in the subsurface and flowing air. Mass transfer effects can curtail the effectiveness of SVE in many settings, and those processes have been widely investigated (Kaleris, 2002; Yoon et al., 2002; Murdoch, 2000; Fischer et al., 1998; Rathfelder et al., 1996; Gierke et al., 1990; Brusseau, 1991).

Low flow rates to wells have long been recognized as critical impediments to the successful use of SVE in low permeability formations (USEPA, 1991). Materials with low gas-phase permeability will inhibit flow and can markedly reduce the effectiveness of SVE, in some cases increasing costs of remediation by orders of magnitude or more (Gierke, 2000; Pederson and Fan, 1992).

Low permeability skin enveloping a well screen is widely recognized as an important factor reducing the effectiveness of wells recovering water, petroleum, or natural gas (Driscoll, 1986; Van Everdingen, 1953). Likewise, low permeability skins enveloping SVE wells could similarly reduce removal rates. Skin on SVE wells appears to have attracted little attention from investigators, and there is scant information available on this effect. This oversight is noteworthy because significant costs can be associated with the efficiency of SVE systems, and an important effort has already been put forth to develop methods for optimizing the performance of SVE (Sun and Yeh, 1998; Sawyer and Kamakoti, 1998; Parker and Islam, 1997; Sun et al., 1996; Sacks et al., 1994; James, 1994; Katyal and Parker, 1993; Amir and Abdul, 1993).

Although well skin can inhibit SVE performance, sand–filled hydraulic fractures can increase the discharge from SVE wells and increase the radius of pressure influence during gas pumping tests (Wolf and Murdoch, 1993). Hydraulic fractures have been used with SVE wells at dozens of contaminated sites, and the results suggest that they can increase contaminant recovery by several times to an order of magnitude or more, largely by increasing the volumetric rate of air flow through the subsurface (Murdoch et al., 1994; Leach et al., 1994; Frank and Barkley, 1994).

Hydraulic fractures are created by injecting fluid into a wellbore. A fracture is nucleated when the injection pressure exceeds some critical value. During hydraulic fracturing, sand is mixed with the injection fluid to form a slurry that fills the fracture as it propagates away

from the wellbore. The fracture closes as the liquid phase of the slurry leaks into the formation, but the sand remains to form a permeable layer that can improve well performance.

Geometries of sand-filled hydraulic fractures can range from flat-lying disks to steeply dipping sheets. Many fractures created in the vadose zone dip gently toward their parent borehole to form crude bowl-shaped features (Murdoch, 1995; Murdoch and Slack, 2002). Dips of these shallow fractures are commonly less than 20°, and the geometry has been idealized as a flat-lying disk to facilitate mechanical analyses (Murdoch, 2002).

Fractures created by injecting compressed gases (pneumatic fractures), or detonating explosives, will also increase the performance of wells. Increases in discharge by an order of magnitude or more have been documented in a variety of applications (Schuring, 2002; Liskowitz et al., 1994; Schuring et al., 1991).

Despite strong empirical evidence that fractures created in the vicinity of well bores will increase the discharge of SVE wells (Murdoch et al., 1994; Schuring, 2002), theoretical analysis of this problem has been limited. A detailed transport analysis by Schulenberg and Reeves (2002) has recently shown that hydraulic fractures can increase the rate of contaminant recovery from low permeability materials. Their sensitivity analysis shows that mass transfer between mobile and immobile phases is important when hydraulic fractures are used, just as when conventional wells are used for SVE. They also show that the properties of the hydraulic fractures themselves will significantly affect the total discharge rates of wells and the rate at which contaminant mass is recovered. Well discharge and contaminant recovery rates are particularly sensitive to the effective transmissivity of hydraulic fractures, which Schulenberg and Reeves (2002) represent by averaging the properties of fractures and matrix by volume within a grid block. They found that recovery rates are less sensitive to changes in fracture length than to changes in transmissivity. Additional analyses of induced fractures during SVE are summarized in reviews by Schuring (2002) and Murdoch et al. (1994).

The objective of this study is to characterize the effects of well skin and sand-filled hydraulic fractures on the flow of air to a SVE well. Effects of contaminant transport have been intentionally avoided to highlight processes that affect the total volumetric discharge.

The approach taken by this paper is to first evaluate using theoretical analyses the problem of pressure and flow in the vicinity of an SVE well with a skin. The analyses will then be extended to evaluate effects of intersecting a hydraulic fracture on well performance. The theoretical analyses are validated using field data obtained from gas-phase pumping tests in the vicinity of clusters of conventional wells in saprolite in western South Carolina. Data from pumping tests conducted using wells intersecting hydraulic fractures will also be evaluated.

2. Theoretical methods

Gas flow to shallow vapor extraction wells reached steady state quickly during our field tests, so following the approach of Mohr and Merz, 1995, Falta et al. (1993) Amir and

Abdul (1993), Shan et al. (1992), Johnson et al. (1990), the early transient pressure response is ignored and only steady conditions are considered. The steady-state distribution of gas pressure in a porous media is assumed to satisfy

$$\nabla \cdot \left(\tilde{k} \nabla P^2\right) = 0 \tag{1}$$

where $\tilde{k}$=gas permeability tensor, and P=gas pressure. Darcy's Law is assumed to be valid for gas flow, and the gas is assumed to have a constant composition and viscosity under isothermal conditions (Shan et al., 1992). The problem is formulated in 2-dimensional, axisymmetric coordinates with the screened interval of the well represented as a line sink, where the depth to the center of the screen is d and its length is L (Fig. 1).

Boundary conditions consist of atmospheric pressure, P_{atm}, at the ground surface, $z=0$, and at a radius of $r=\infty$. A horizontal no-flow boundary is located at a depth of $z=b$, and a vertical no-flow boundary is at $r=0$ above and below the well screen.

$$P = P_{\text{atm}} \text{ at } 0<r<\infty, z = 0 \tag{2a}$$

$$P = P_{\text{atm}} \text{ at } 0<z<b, r = \infty \tag{2b}$$

$$\frac{\partial P}{\partial r} = 0 \text{ at } 0<z<d - \frac{L}{2}, r = 0 \tag{2c}$$

$$\frac{\partial P}{\partial r} = 0 \text{ at } d + \frac{L}{2}<z<b, r = 0 \tag{2d}$$

$$\frac{\partial P}{\partial z} = 0 \text{ at } z = b \tag{2e}$$

2.1. Solution for an ideal well

An analytical solution to Eqs. (1) (2a)–(2e) is obtained by integrating the point source solution and applying superposition to represent the upper and lower boundary conditions. The result gives the pressure in the formation as

$$P_1(r,z) = \sqrt{P_{\text{atm}}^2 - C_1 \lambda(r, z, k_{\text{r}}, k_{\text{z}}, L, d, b)} \tag{3a}$$

$$C_1 = \frac{P_{\text{atm}} Q_{\text{s}} \mu}{2\pi L k_{\text{r}}} \tag{3b}$$

where Q_{s} is the volumetric flow at standard pressure and temperature, μ is fluid viscosity, L is the length of the well screen, and k_{r} is horizontal permeability. The term $\lambda(r,z,k_{\text{r}},k_{\text{z}},L,d,b)$ is given in Appendix A or in a slightly different form by Shan et al. (1992, Eq. 20).

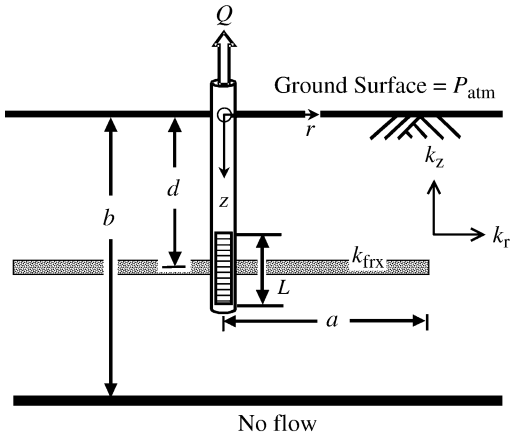

Fig. 1. Configuration and dimensional specifications of conventional well and sand-filled hydraulic fracture used in the analysis.

2.2. Including skin

The process of creating a well may result in a *skin* of different permeability material around the well screen. The pressure in a recovery well will be less than that in the formation because of energy losses during flow through the skin (Arps, 1955; Van Everdingen, 1953). The pressure loss across a skin enveloping a conventional SVE well can be determined by assuming the flow through the skin is horizontal and is one-dimensional in a radial direction. Integrating the one-dimensional form of Eq. (1) in radial coordinates and using the boundary conditions

$$P = P_1 \text{ at } r = r_s \tag{4a}$$

$$\frac{dP}{dr} = \frac{Q_s \mu P_{atm}}{2\pi L r_s k_s P} \text{ at } r = r_s \tag{4b}$$

where r_s is the radius of the skin, will give the pressure in an SVE well with a skin as

$$P(r_w) = \sqrt{P_1(r_s, d)^2 - 2C_1\sigma} \tag{5}$$

where the skin factor, σ, is (Earlougher, 1977)

$$\sigma = \left(\frac{k}{k_s} - 1\right)\ln\left(\frac{r_s}{r_w}\right) \tag{6}$$

This gives positive values of σ where the skin consists of low permeability material, and negative values of σ where the skin is relatively high permeability material.

2.3. A well intersecting a hydraulic fracture

A well intersecting a sand-filled hydraulic fracture will be simulated using a finite difference solution to Eq. (1). The finite difference solver uses Gauss–Seidel iteration and successive over relaxation with a convergence tolerance of 10^{-6} (Wang and Anderson, 1982). The dimensions of the model were set to resemble conditions at our field sites, but they are representative of many shallow applications. The bottom boundary is at $b=8$ m (the depth of the water table at the site), and a no-flow boundary is set at $r=20$ m. The fracture is represented as a thin disc whose permeability is greater than that of the formation. A depth of $d=3.0$ m and radius of $r=4.2$ m are used as baseline values for most calculations, but other depths and sizes of fractures are evaluated. One or several grid blocks are held at constant pressure to represent the screened interval of the well (Fig. 1).

A finite-difference grid was designed to be accurate with reasonable execution time. This design was accomplished using closely spaced cells in the vicinity of the well screen and the fracture and more widely spaced cells elsewhere in the grid. The first 10 columns closest to the well have a uniform spacing of 0.01 m, and then a geometric progression is used to increase the widths of the columns with increasing distance from the well. A row spacing of 0.01 m was used to represent the fracture, which is the thinnest row used in the grid. The row height was increased using a geometric progression upward to the ground surface, and another geometric progression downward to the base of the model.

A hydraulic fracture of varying thickness was represented using a grid layer of constant thickness by varying the horizontal and vertical permeability. This was done using the thicknesses and permeabilities of the fracture and the matrix in each the grid block, and applying arithmetic and harmonic averages commonly used for calculating effective anisotropic conductivities of layered media (Fetter, 2001, p. 105).

Streamlines for conventional wells were determined by contouring the stream function calculated using methods of Shan et al. (1992) and given in Appendix A. Streamlines were calculated for the numerical solutions by first integrating the vertical flux at the ground surface from the well to the outer edge of the model to determine the radially cumulative inflow rate at the ground surface. The starting point for each streamline was located where the cumulative flow rate was equal to multiples of one-tenth of the total flow. Streamlines were then determined by integrating the velocity field from the starting location to the well (Pollock, 1988).

The numerical solution was verified by comparing results to the analytical solution described above. Relative errors in the pressure calculation were determined along three representative vertical lines. The maximum relative error between the numerical and analytical solutions is 0.031 and it occurs at a depth of 2.9 m and r=0.065 m. This is slightly above the top of the well screen. The average error along that column is 0.008. The maximum error along the other vertical profiles occurs at a similar depth, but is less than the error at $r=0.065$ m (Bradner, 2002).

The streamlines calculated numerically were compared to contours of the analytical solution for the stream function. A convergence criteria of 10^{-8} was required to obtain sufficient accuracy for the numerical streamline calculations. The results show that the streamlines follow similar paths for the two solutions (Fig. 2). The greatest error occurs at

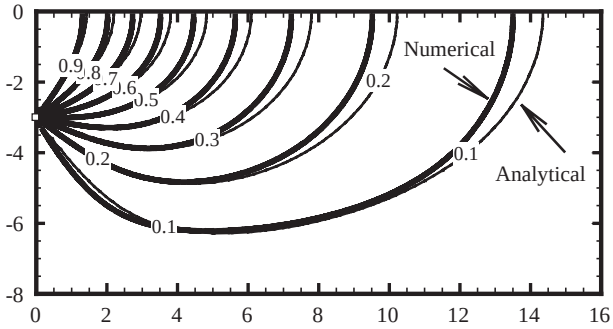

Fig. 2. Stream function in the vicinity of a vertical well determined by contouring analytical solution (thin lines) and using a numerical procedure (thick lines).

the ground surface where the streamlines determined analytically lie as much as 6% further from the well than the numerically determined streamlines. The pairs of streamlines converge and are nearly identical over roughly two thirds of their total length. The error near the ground surface is related to the convergence criteria and the grid size at the ground surface. The error can be reduced by decreasing the convergence criteria and increasing the number of points in the grid.

3. Results of theoretical analyses

Well performance can be evaluated using simple scalar measures or through multi-dimensional plots of fields of pressure and flowpaths. Specific capacity is a scalar measure that has been used to characterize the performance of water wells and oil production wells (Driscoll, 1986; Fetter, 2001; Earlougher, 1977), although this approach has apparently seen limited application for SVE wells. Using the analytical solution for the performance of an SVE well, it follows that the *specific gas capacity* of a well is

$$S_c = \frac{Q_s}{\left(P_{atm}^2 - P_{well}^2\right)} \tag{7}$$

where Q_s is the volumetric discharge scaled to standard pressure, P_{atm} is atmospheric pressure, and P_{well} is the pressure at the well screen. This form differs slightly from the equivalent term used to characterize water wells or oil wells where the denominator of Eq. (7) is replaced with drawdown.

Specific gas capacity depends on the geometry of the well and boundary conditions, and the gas phase permeability of the formation. The specific gas capacity is expected to be constant over a moderate range of flowrates and pressures at the well, which is consistent with our field observations. Presumably, S_c changes at high suctions when the Klinkenberg effect becomes important (Klinkenberg, 1941), but at values of suction typical of most field implementations of vapor extraction, S_c is expected to be constant.

It is convenient to evaluate performance of a well by scaling the actual gas capacity, S_c, to the specific gas capacity of an ideal control well unaffected by skin, S_{co}. The ratio

$$F = \frac{S_c}{S_{co}} \tag{8}$$

is referred to as *flow efficiency* following terminology used in the petroleum industry (Earlougher, 1977; Streltsova, 1988).

3.1. Analysis of vertical wells with skin

A low permeability skin on a conventional vertical well will cause the flow efficiency to be less than 1.0, and this effect can be determined for an idealized well according to

$$F = \frac{\lambda(r_w, d, k_r, k_z, L, d, b)}{\lambda(r_w, d, k_r, k_z, L, d, b) + 2\sigma} \tag{9}$$

where $\lambda(r,z,k_r,k_z,L,d,b)$ is used in Eqs. (3a) and (3b) and defined in Eq. (A3), but in Eq. (9), it is evaluated at the center of the well screen. In general, F decreases gradually for increasing positive values of skin factor but it increases markedly for decreasing values of negative skin factor. It is apparent that $F \rightarrow \infty$ as $\sigma \rightarrow -0.5\ \lambda(r,z,k_r,k_z,L,d,b)$, and the practical lower limit of the skin factor will be bounded by this singularity. For example, SVE wells used during our field work have the following characteristics: $b = 3$ m, $d = 8$ m, $r_w = 0.05$ m, $L = 0.3$ m, which gives a value of $\lambda = 3.59$. The lower limit of the skin factor is $\sigma = -1.79$ for these wells.

A sensitivity analysis shows that increasing the length of the screen increases flow efficiencies where wells are adversely affected by skin ($\sigma > 0$), and decreases flow efficiency where well skin improves recovery ($\sigma < 0$) (Fig. 3). Changing the depth of the well screen has a negligible effect on how well skin affects flow efficiency, as indicated by the superimposed curves in Fig. 3.

Anisotropy in the formation also affects how a skin will influence well performance (Fig. 3). For conditions where $k_v < k_h$, such as where horizontal stratification is important, the flow efficiency increases where skin adversely affects flow ($\sigma > 0$) compared to isotropic conditions. Where skin enhances flow to the well ($\sigma < 0$), the flow efficiency in horizontally stratified formations is diminished compared to the isotropic case. The effect is reversed in formations where $k_h < k_v$, such as where vertical fractures are important. In this case, F decreases for $\sigma > 0$ and increases for $\sigma < 0$ compared to the isotropic control (Fig. 3b).

Well radius is also a control of flow efficiency of an SVE well affected by skin. Flow efficiency generally increases with well radius, and the effect is particularly strong for relatively narrow wells (e.g., $r_w < 5$ cm; Fig. 4).

The effects of screen length, anisotropy, and well radius appear to be a result of how those factors affect the flux through the skin. Increasing screen length or well radius will decrease the flux through the skin for a given well discharge, and this will diminish the effect of a skin. Increasing the ratio k_v/k_h is similar to lengthening the problem domain in the vertical direction and conducting the analysis in isotropic

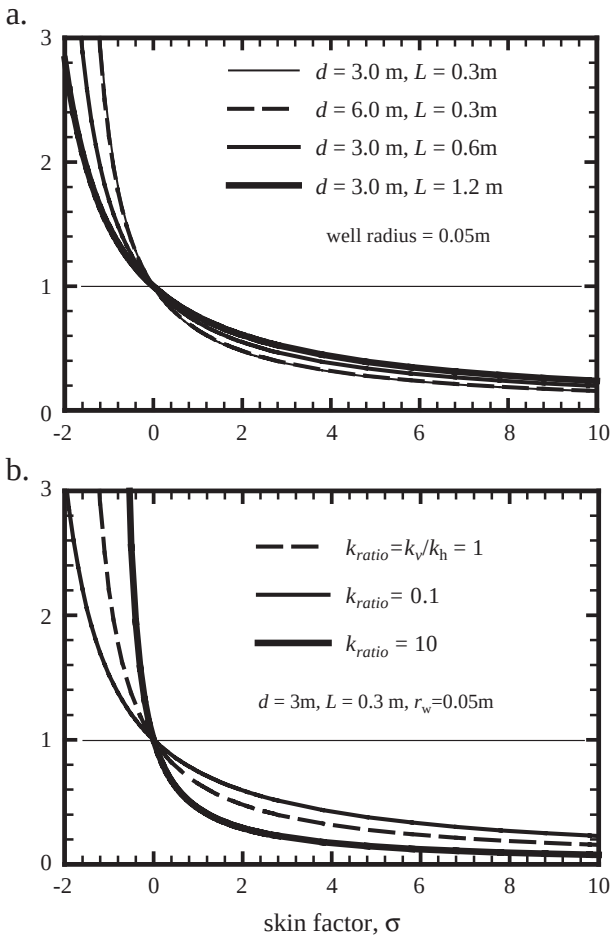

Fig. 3. Flow efficiency of a conventional well as a function of skin factor for different (a) well lengths; and (b) anisotropies.

conditions (Shan et al., 1992). Increasing k_v/k_h effectively reduces the flux through the skin for a given volumetric discharge, so the effect will be similar to lengthening the screen. Of course, the coordinate transform also increases the depth of the well in isotropic space, but this has negligible effect on the role of skin because it does not affect flux.

Decreasing the conductance of the skin, by either increasing thickness or decreasing permeability, can markedly reduce well performance (Fig. 4). The performance of a well with a skin 5 mm thick and composed of material with a permeability 10 times less than the formation will be reduced to 0.6 to 0.75 of the ideal performance, depending on well radius (Fig. 4). Increasing the permeability contrast to 100 cuts the flow efficiency to 0.1 to 0.2, assuming the thickness remains 5 mm. Even if the

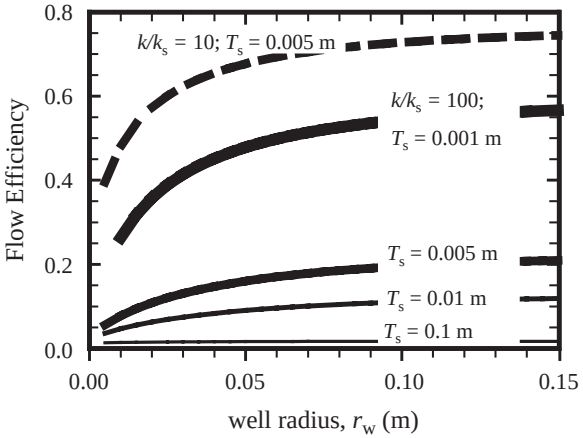

Fig. 4. Flow efficiency for a conventional SVE well as functions of well radius, skin thickness, T_s, and the ratio of formation to skin permeability, k/k_s. $d=3.0$ m.

thickness of the skin is only 1 mm, the flow efficiency is 0.5 where the contrast in permeability is 100 (thickest line in Fig. 4).

3.2. Analysis of wells intersecting hydraulic fractures

The performance of wells intersecting hydraulic fractures was evaluated by determining flow efficiencies and pressure and stream function fields for a variety of idealized scenarios similar to field conditions. Hydraulic fractures were represented as flat-lying disks with permeabilities exceeding those of the formation. Some fractures were represented as disks of uniform thickness and permeability, whereas others were represented as features whose aperture diminishes with distance from the well. In all cases, flow efficiencies were determined by scaling discharges from the heterogeneous models representing hydraulic fractures to discharges calculated using the same boundary conditions but with isotropic and homogeneous material.

The simplest representation of a hydraulic fracture is a disk of radius R and uniform aperture, δ, at a depth, d, and filled with material of permeability k_{frx}. A baseline case of $R=4.2$ m, $d=3$ m, and $\delta=5$ mm is used. A sensitivity analysis was conducted to evaluate how flow efficiency is affected by the ratio between the permeability of the fracture and the formation, $k_r=k_{frx}/k$, and other factors related to the geometry of the fracture and well.

Results of the sensitivity analysis (Fig. 5) show that F increases with k_r, but the effect is minor for $k_r<10$, and only where $k_r>50$ is $F>2.0$. Increasing k_r produces larger values of F, and $k_r>500$ is required for $F>10$, assuming parameters for the baseline case. This implies that the material in the fracture must be at least 50 times more permeable than the formation to double the specific gas capacity of the well, but a contrast in permeabilities of 500 will increase S_c by a factor of 10 ($F\geq 10$).

The flow efficiency is independent of fracture radius for $k_r<200$, but F increases with R for $k_r>200$ (Fig. 5). Interestingly, even the relatively small radius of $R=1.0$ m

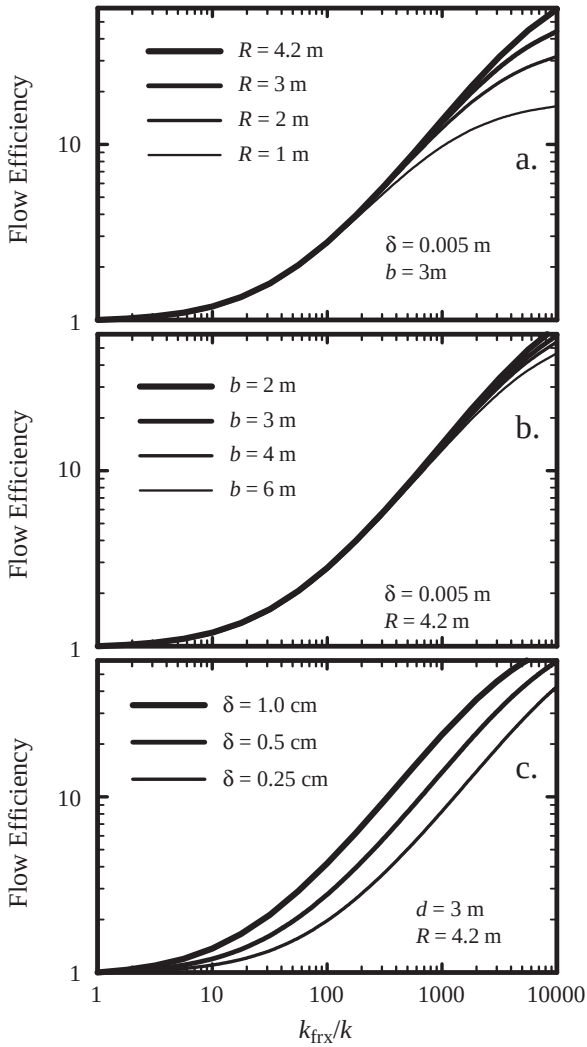

Fig. 5. Flow efficiency for an SVE well intersecting a disk-shaped hydraulic fracture of uniform aperture as functions of the ratio of fracture to formation permeability, k_{frx}/k, and (a) fracture radius, (b) depth, and (c) aperture.

produces a 10-fold increases in well performance where $k_r = 1000$. It is probably impractical to make a hydraulic fracture at a depth of 3 m whose radius is significantly greater than roughly 5 m (Murdoch, 2002), so 4.2 m was used as a conservative estimate of the largest radius.

The depth of the fracture has only a minor effect on F for a fracture with a radius of 4.2 m and an aperture of 0.005 m. The effect of depth is negligible where $k_r < 1000$, but the flow efficiency is greater for shallow fractures compared to deep fractures where $k_r > 1000$ (Fig. 5b).

Aperture is the most important of the three fracture geometry variables, affecting the flow efficiency over the entire range of k_r for a fracture at a depth of 3.0 m with a radius of 4.2 m (Fig. 5c). Clearly, increasing the aperture of a uniform fracture will have a major effect on well performance, which is consistent with the findings of Schulenberg and Reeves (2002).

Apertures of sand-filled hydraulic fractures can be highly variable over short distances, but they typically are thickest in the vicinity of the well bore and taper toward their distal edge (Murdoch and Slack, 2002; Richardson, 2003). The aperture can be predicted using methods based on fracture mechanics and given in Murdoch (2002) and Bradner (2002). This provides a way to relate the aperture and length of a hydraulic fracture to the volume of sand injected into the fracture, a quantity known from field records. Fracture aperture distributions were determined from mechanical analysis (Eqs. (73) and (74) in Bradner, 2002) and then those data were used to calculate flow efficiency. The results indicate that the flow efficiency increases as a function of injected sand volume and permeability ratio, and a plot of the data resembles Fig. 5c and is not given here (it is given in Bradner, 2002; Fig. 32). This method of combining mechanical analysis of fracture growth with analysis of flow efficiency holds promise for designing hydraulic fractures used for SVE.

3.3. Pressure field and streamlines

Flow efficiency and specific gas capacity are important scalar measures of well performance, but some applications require insight into the patterns defined by pressure and flow fields in the subsurface (Falta et al., 1993). Gas pressure in the formation, P, was calculated using the numerical model and normalized to $P_{well}=0.9$ atm, which is the pressure at the well during the simulation. The normalized pressure is $P_d=(P_{atm}-P_{obs})/(P_{atm}-P_{well})$. The normalized pressure that can be resolved on contour plots (Fig. 6) ranges from 0.01 to 0.50 because larger dimensionless pressures are obscured by closely spaced contour lines in close proximity to the well. Fields of dimensionless pressure and streamlines (Fig. 6) were calculated for fractures with uniform thickness and radius ($\delta=5$ mm, $a=5$ m) and filled with materials of different k_r. Pressure fields and flowlines in the vicinity of fractures filled with different volumes of sand (variable aperture determined using mechanical analyses) resemble the results shown in Fig. 6 and are given in Bradner (2002; Fig. 34).

Changes in gas pressure are confined to the proximity of the conventional well (shown as $k_r=1.0$ in Fig. 6). For convenience, we will define the radius of pressure influence as the radial distance where $P_d=0.1$ at the depth of the center of the well screen (the radius of effective remediation produced by this well may differ from this definition of radius of influence). The radius of pressure influence is located a few tenths of a meter away from the extraction well in this example (Fig. 6). A fracture where $k_r=100$ results in a pressure distribution that is broadened slightly, and the radius of pressure influence is extended to 1.2 m where it cuts through the fracture itself. More striking changes occur where $k_r=1000$. The pressure field is intensified significantly around the fracture, and the radius of pressure influence is increased to 5.0 m,

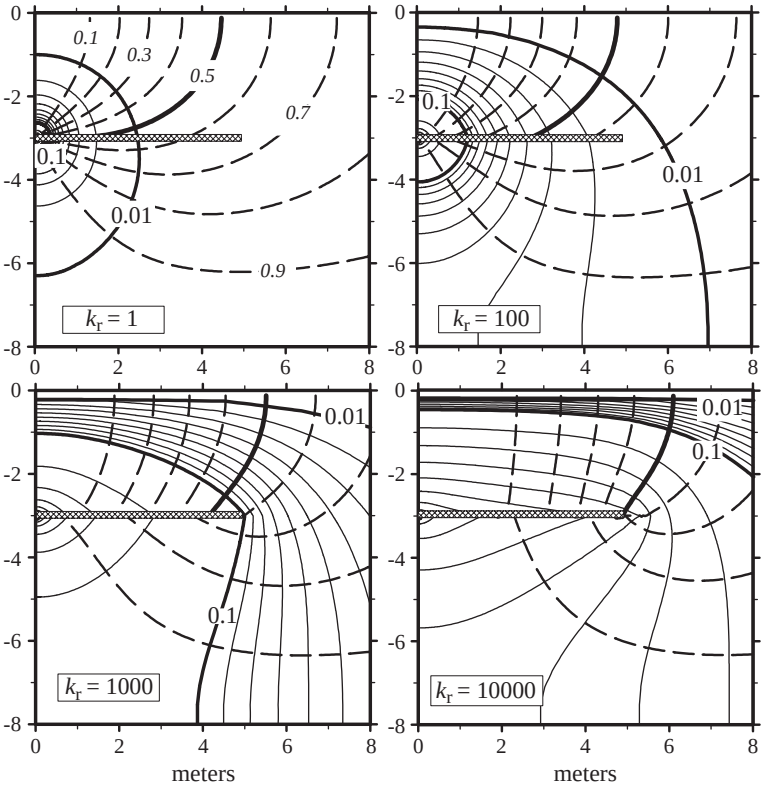

Fig. 6. Normalized pressure contours in log scale (solid lines) and streamlines (dashed lines) for varying ratios of fracture sand permeability and formation permeability, k_r. 50% streamline is the thick solid line.

approximately equal to the radial extent of the fracture. Increasing the permeability of the fracture relative to enveloping material even more, to $k_r = 10,000$, advances the radius of pressure influence to 8.0 m.

Streamlines to conventional wells and wells intersecting hydraulic fractures are vertical at the ground surface and curve to converge on the well screen. The general effect of increasing k_r is to steepen the streamlines at shallow depths overlying the fracture, and to broaden the distribution of flow. The distribution of flow can be highlighted by the location of the 0.5 streamline, shown as a bold line in Fig. 6. This streamline defines a bowl-shaped surface that envelops a region through which half of the discharge of the well will flow. The radius of this bowl-shaped region is greatest at the ground surface where it is equal to 4.5 m for a conventional well with a short screen at 3.0 m depth (Fig. 6). The radius of the 0.5 contour increases to 4.8 m where $k_r = 100$ and 6.0 m where $k_r = 10,000$.

The pattern of streamlines can be scaled to the depth of the well, so it appears that the 0.5 streamline intersects the ground surface at a radial distance of approximately 1.5 times the depth of a conventional well, whereas it intersects the ground surface at a radial

distance as far as 2.0 times the depth of a well intersecting a flat-lying hydraulic fracture in an isotropic medium.

4. Field tests

Field experiments were conducted at two sites at the northern and southern ends of the Simpson Agricultural Experimental Station, 5 km west of the town of Pendleton in Anderson County, western South Carolina. The north site is underlain by granitoid gneiss, and the south site by biotite schist (Nelson et al., 1990). Bedrock at both sites is overlain by at least 15 m of saprolite, which is overlain by 2 to 3 m of massive sandy, clayey silt typical of the B soil horizon. Similar profiles are common throughout the Piedmont physiographic province (Sowers and Richardson, 1983). Relic banding and schistosity in saprolite at the site are roughly flat-lying (dips less than 10°), according to core samples at both sites.

Field tests were conducted using shallow wells, 3.0 m deep or shallower, so only the upper part of the saprolite and the B soil horizon are relevant to the tests. The contact between the saprolite and the B-horizon is irregular and typically occurs from 2.0 to 2.5 m, although the contact is locally as deep as 4 m or more. Both the saprolite and the B-horizon consist of quartz, mica, clay, and iron oxides. Relic structures and texture derived from the underlying crystalline rock are preserved in the saprolite and are highly variable, whereas the B-horizon is massive sandy, clayey silt, containing bands and pods of quartz and mica derived from weathered pegmatite.

Soil samples were taken at 0.3-m intervals to a depth of 3.0 m with a split-spoon, and additional samples were taken with a Shelby tube and used to determine basic properties (Table 1). The B-horizon differs slightly from underlying saprolite in most basic properties. Porosity is generally in the range of 0.40 to 0.45 within the B-horizon, and it increases to 0.48 to 0.50 in the underlying saprolite. The volumetric

Table 1
Soil properties as a function of depth at the north site

Depth (m)	Bulk unit weight (kg/m3)	Grain size fraction <0.075 mm	Porosity	Volumetric moisture content	Degree of saturation	Gas-phase permeability $\times 10^{11}$ m^2	Suction head (m)	USCS	Soil horizon
0.3	1504	0.41	0.41	0.20	0.7		4.84	SM	A
0.6	1113		0.56	0.23	0.41		4.06	SM\MH	E\BE
0.9	1534	0.48	0.4	0.31	0.77	28	2.60	SM\MH	Bt
1.2	1423	0.52	0.44	0.31	0.7	28	3.40	SM\MH	Bt
1.5	1463		0.43	0.39	0.92	0.35	2.44	SM\MH	Bt
1.8	1413	0.30	0.45	0.44	0.99	0.35		SM\MH	Bt
2.1	1494		0.42	0.40	0.96	0.005		SM\MH	Bt
2.4	1333	0.27	0.48	0.47	0.98	0.005		SM\MH	BC
2.7	1323		0.48	0.34	0.7	0.27		SM	C
3.0	1213	0.2	0.52	0.43	0.82	0.1		SM	C
Ave	1381	0.36	0.46	0.35	0.80	7.1	3.46		
S.D.	136	0.13	0.05	0.09	0.18	13.0	1.00		

moisture content increases with depth in the B-horizon, from 0.20 at 0.3 m to 0.47 at 2.4 m. Moisture decreases abruptly to 0.34 when crossing the contact into underlying saprolite. As a result, the degree of saturation increases with depth to nearly 1.0 at the bottom of the B-horizon, but it decreases to 0.70 to 0.82 within the saprolite (Table 1).

4.1. Methods

Each experimental site consists of a cluster of conventional wells, wells intersecting sand-filled hydraulic fractures, and piezometers. The north site includes a cluster of 10 conventional wells installed using several different drilling methods and spaced roughly 0.3 m apart within a 2.0 m^2 area. The cluster at the south site contains seven wells within 3.0 m^2.

Hydraulic fractures were created by injecting sand-laden slurry into 2-inch (nominal) steel pipe pushed to a depth of 3.0 m. Techniques for creating hydraulic fractures are described in Richardson (2003), Murdoch and Slack (2002), and Murdoch et al. (1994). Four hydraulic fractures were created at the field sites: two fractures at the north site and two at the south site. Each site contains one fracture filled with medium-grained sand and one filled with coarse-grained sand. The permeabilities of the medium-grained and coarse-grained sand are 2×10^{-10} m^2 and 6×10^{-10} m^2, respectively. Sand was transported into the fractures using between 600 and 850 l of guar gum gel, a cellulose-based compound mixed with water. An enzyme was added to break down the gel after injection. SVE testing was conducted more than 6 months after the fractures were created and there was no evidence of the gel in samples of the sand obtained using a split spoon at this time.

Gas pumping tests were conducted using a 1 hp, 50 Hz rotary vane blower. Gas flow rates were measured using three variable area flow meters, with maximum flow rates of 1, 10, and 40 standard ft^3/min. The accuracy of the flow meters is 2 to 5% of full scale. Pressure was measured using two Dwyer Mark III digital manometers, with maximum pressures of 5 kPa and 50 kPa and accuracies of 1% of full scale. The accuracy of field measurements was maximized by selecting a meter whose full scale was closest to, while still exceeding, a particular measurement.

Wells with a conventional design were used for both gas pumping and as pneumatic piezometers. Borings for the wells were created using three different devices, which created different diameter holes: hand augers (5.7 cm); machine augers on a drilling rig (10.2 cm); and shelby-tubes (7.6 cm). A single pass of a cylindrical nylon brush slightly larger than each bore diameter was used in an effort to remove smeared material from the borehole walls. The completion consists of 0.3 m of pea gravel at the bottom of the boring, overlain by 0.15 m of bentonite and then non-shrink cement to the ground surface. Half-inch PVC pipe extends from the ground surface to the mid-depth of the gravel.

It was important to seal the sand pack using a mixture of powdered and granular bentonite that is hydrated by slowly trickling in a few 10s of ml of water. Aggressively hydrating the bentonite could cause the gravel to fill with water, and failing to hydrate the bentonite could cause the gravel to fill with cement, both of which would adversely affect performance of the piezometer or well. An additive (Tetraguard AS-20) was used to reduce the water required to hydrate the cement, which in turn reduces the shrinkage of the

cement. Most of the conventional wells were completed at a depth of 3.0 m, and a few were completed at 1.5 m.

Piezometers created using the design outlined above with 0.3-m-long gravel sections produce rather poor resolution of pressure measurements, so multi-level piezometers with shorter screens were also used. Multi-level piezometers were created by pulling a bundle of vinyl tubes (3.2 mm o.d.) into a sleeve of 0.1 mm-thick (4 mil) lay-flat polyethylene. Each tube terminated at a small brass elbow fitting (Clippard Minimatic), which was fastened through the poly sleeve as a bulkhead fitting. A filter formed from Scotchbrite abrasive pad approximately 4 cm on a side and 4 mm thick was attached to the outside of the elbow fitting where it contacted the formation and prevented clogging of the orifice in the fitting. Measurement ports and filters were spaced approximately every few tenths of a meter along the sleeve.

A weight was attached to the bottom of the sleeve and it was lowered into a borehole created by continuously removing core samples with a split spoon (the borehole wall was brushed once to disrupt smeared material). The sleeve was inflated initially with air, and then it was filled with dry sand to hold it in place during operation. This multi-level completion was remarkably inexpensive, easy to deploy, and seemed to provide accurate pressure measurements. Additional details are described by Bradner (2002), and the basic approach we used is patterned after Jones et al. (1999).

The pipe used to create the hydraulic fractures served as the extraction well during vapor extraction tests. Multi-level piezometers were the primary tool for obtaining pressure distributions in the vicinity of wells intersecting fractures. A few conventional wells were also installed near the fracture to evaluate reliability of data from the multi-level piezometers.

Gas pumping tests were conducted in the conventional well clusters using each well for extraction, with the others used as pneumatic piezometers. Each of the 10 tests at the north site generated a flow rate and pressure measurement at the well and 9 pressure measurements at piezometers, and each of the 5 tests at the south site generated data from the well and 4 piezometers. In addition, pumping tests were conducted at the two wells intersecting fractures at each site. Pressures were measured at multi-level and single-level piezometers in the vicinities of the fractures.

Local formation permeabilities were obtained in the field using shelby-tube column tests. Soil samples were taken in 0.6 m increments to a depth of 3.66 m. Shelby-tubes filled with sample were attached to an air injection head fitted with a pressure transducer. One end of the sampler was left open to the atmosphere, while the other was sealed with the injection head. Air was injected into the shelby-tube at various flow rates and the corresponding pressure was used to calculate the gas permeability (Bradner, 2002).

4.2. Conventional vertical wells

Several tests were conducted by progressively closing a valve to decrease the flow rate and then measuring the flow rate at the conventional well. Standard volumetric discharge was correlated with $(P_{\mathrm{atm}}^2 - P_{\mathrm{well}}^2)$, and the Pearson product moment correlation coefficients, r, ranged from 0.993 to 0.997 over the range of the blower ($P_{\mathrm{well}} > 91$ kPa). The strong correlation (Bradner, 2002; Fig. 27) validates the use of the specific gas

capacity, S_c (Eq. (7)), to characterize well performance, at least within the ranges of pressures produced by the blower we used.

Specific gas capacities of wells within the conventional well clusters range over an order of magnitude (Table 2). At the north site, S_c ranges from 0.10 to 1.56 m^3s^{-1} MPa^{-2} (2.2 to 33.8 scfm atm^{-2}), the arithmetic mean is 0.53 m^3s^{-1} MPa^{-2}, and the geometric mean is 0.028 m^3s^{-1} MPa^{-2}. Volumetric rates in S_c are scaled to standard pressure. Specific gas capacities at the south site are greater than those at the north site, but they too are quite variable. They range from 0.91 m^3s^{-1} MPa^{-2} to 5.5 m^3s^{-1} MPa^{-2} (19.7 to 118.9 scfm/atm^2), with an arithmetic mean of 2.9 m^3s^{-1} MPa^{-2} and a geometric mean of 2.2 m^3s^{-1} Pa^{-2}.

Formation permeabilities were estimated by correlating pressures observed at piezometers with pressures predicted using Eqs. (3a) and (3b), which assumes that the formation is homogeneous and anisotropic. This approach to estimating gas phase permeability is similar to that used by Olson et al. (2001), Chen (1997), Edwards and Jones (1994), Shan et al. (1992), and Baehr and Hult (1991).

The data from the multiple pumping tests were analyzed two ways. One method was to analyze all the pumping tests conducted on conventional wells at a site simultaneously as an ensemble. This will be termed the *ensemble* analysis. The other method is to analyze each test individually, and then combine the results as average values. This will be termed the *individual* analyses.

Correlation coefficients for the ensemble analyses were calculated for ranges of k_v and k_h that bracket optimal values. A maximum correlation coefficient of 0.930 was obtained when data from all 10 tests at the north test (90 pressure measurements) were analyzed as

Table 2
Performance of conventional and fractured wells and north and south sites

Well	Well type	S_c $m^3s^{-1}MPa^{-2}$	Average S_c by well type	Flow efficiency	Average F by well type	Skin σ
NW-1	Machine auger	0.11		0.04		25
NW-2	Machine auger	0.10		0.03		26
NW-10	Machine auger	0.13		0.04		21
NW-6	Machine auger	0.11	0.11	0.04	0.04	25
NW-7	Shelby tube	0.22		0.07		12
NW-8	Shelby tube	0.40	0.31	0.14	0.11	6.0
NW-3	Hand auger	1.56		0.54		0.84
NW-4	Hand auger	1.32		0.45		1.1
NW-5	Hand auger	0.10		0.03		26
NW-9	Hand auger	1.28	1.1	0.44	0.37	1.2
NFCRS	Fracture, crs grain	9.2		3.2		−0.37
NFMED	Fracture, med. grain	14.6	12	5.0	4.1	−0.44
SW-4	Machine auger	1.0	1.0	0.27	0.27	5.1
SW-1	Hand auger	0.91		0.25		6.0
SW-2	Hand auger	5.2		1.4		−0.54
SW-3	Hand auger	5.5		1.5		−0.63
SW-5	Hand auger	1.9	3.4	0.52	0.93	1.8
SFCRS	Fracture, crs grain	17.7		4.9		−1.3
SFMED	Fracture, med grain	12.0	15	3.3	4.3	−1.2

an ensemble using $k_h = 0.52 \times 10^{-11}$ m^2, $k_v = 3.8 \times 10^{-11}$ m^2 (Table 3). Those permeabilities were obtained using a Levenberg–Marquardt minimization algorithm, and they produce the best fit to the ensemble data. However, there are many possible combinations of k_h and k_v that produce generally similar correlation with the field data. For example, permeabilities within this range: $0.4 \times 10^{-11} < k_h < 1.4 \times 10^{-11}$; $2 \times 10^{-11} < k_v < 10 \times 10^{-11}$ can be selected to produce $r > 0.9$.

The optimal estimates of permeabilities for the ensemble data at the south site are $k_h = 1.3 \times 10^{-11}$ m^2, $k_v = 1.0 \times 10^{-11}$ m^2, and this produces $r = 0.89$ (Table 3). However, permeabilities within this range: 1.0×10^{-11} m$^2 < k_h < 2.0 \times 10^{-11}$ m^2; 0.5×10^{-11} m$^2 < k_h < 1.5 \times 10^{-11}$ m^2 can be selected to give $r > 0.85$. Only certain pairs of permeabilities within that range will give $r > 0.85$, whereas others will give much poorer correlation. Specific values of permeabilities that will give $r > 0.85$ are given in Bradner (2002; Fig. 41). In analyses that follow, we will use values of permeability given above as optimal correlations between observations and predictions, but it is important to recognize that a range of permeabilities will give values of correlation that are only slightly less than optimal.

Interpreting results from the theoretical analyses requires determining k_{frx}/k, which requires characterizing the average gas-phase permeability assuming isotropic conditions, k. The results are $k = 1.5 \times 10^{-11}$ m^2 for the north site and $k = 1.1 \times 10^{-11}$ m^2 for the south site (Table 3).

Another approach to analyze the pumping tests is to determine the permeabilities that minimize residuals for each individual pumping test. This gives 10 pairs of permeabilities, k_h and k_v, for the north site and 5 pairs for the south site. These results were then averaged arithmetically and geometrically to produce alternate estimates of average permeabilities (Table 3).

The arithmetic mean overestimates the ensemble values by as much as a factor of 8, but the geometric mean values are more similar to the ensemble values. The correlation between the observed data from all tests and the results predicted using the mean values of permeability is poorer ($0 < r < 0.02$ when using arithmetic mean k, $0.64 < r < 0.83$ for geometric mean k) than when using permeabilities obtained by inverting the ensemble of all the tests. It appears that permeability values estimated by averaging individual pumping tests are a poor substitute for analyzing multiple tests as an ensemble.

Table 3
Permeabilities determined by different methods

Inversion approach	Assumption	North site		South site	
		k_h (m$^2 \times 10^{-11}$)	k_v (m$^2 \times 10^{-11}$)	k_h (m$^2 \times 10^{-11}$)	k_v (m$^2 \times 10^{-11}$)
Ensemble	Anisotropic	0.52	3.81	1.32	1.03
		$r = 0.93$	$r = 0.93$	$r = 0.89$	$r = 0.89$
Ensemble	Isotropic	1.51	1.51	1.15	1.15
		$r = 0.92$	$r = 0.92$	$r = 0.89$	$r = 0.89$
Individual	Arithmetic mean	4.31	4.43	2.87	2.30
		$r = 0.02$	$r = 0.02$	$r = 0.0$	$r = 0.0$
Individual	Geometric mean	0.97	2.72	2.03	1.66
		$r = 0.83$	$r = 0.83$	$r = 0.64$	$r = 0.64$
Individual	Standard deviation	±5.46	±4.62	±2.60[1]	±2.27

Skin factors were determined by first estimating k_h and k_r using pressure data at piezometers, and then using pressure data at the well to determine σ from Eq. (5). Values of skin factor at the north site range from 0.84 to 26, and at the south site they range from −0.6 to 6.0 (Table 2).

Calculating flow efficiency requires determining S_{co} of a conventional well under ideal conditions (Eq. (9)); that is, S_{co} of a conventional well that lacks skin. Values of S_{co} were determined theoretically using the values of k_h and k_v from the isotropic ensemble analysis (Table 2), and using the appropriate diameter for the well. Flow efficiencies calculated using this method for the conventional wells at the north site range from 0.035 to 0.537, and at the south site from 0.250 to 1.507 (Table 2).

4.3. Wells intersecting hydraulic fractures

The specific gas capacity of the well intersecting the fracture filled with medium-grained sand at the north site is 14.6 m^3s^{-1} MPa^{-2}, whereas it is less, 9.2 m^3s^{-1} MPa^{-2}, for the well intersecting the fracture filled with coarse-grained (Table 2). Similar values were observed at the south site, but here S_c of the well intersecting the coarse-grained fracture is greatest, 17.7 m^3s^{-1} MPa^{-2}, and $S_c = 12.0$ m^3s^{-1} MPa^{-2} for the well intersecting medium-grained fracture (Table 2).

Flow efficiencies for the wells intersecting hydraulic fractures range from 3.2 to 5.0, assuming that S_{co} is determined theoretically using values of k_h and k_v from the ensemble analysis (Table 3).

4.4. Pressure distribution

Arrays of piezometers were used to measure pressure distributions in the vicinities of hydraulic fractures and the results of those measurements were compared to predictions using theoretical analyses described earlier. The most complete set of pressure measurements was obtained from the vicinity of the fracture filled with medium-grained sand at the south site. Five multi-level piezometers were created along a radial line and several other single-level piezometers were created at other locations near the fracture.

The numerical model was used to evaluate field observations by considering three different zones of permeability: the fracture itself, an upper layer corresponding to the B-horizon, and a lower layer corresponding to the saprolite. Permeabilities of these units were initially set at values obtained from lab and field permeability tests, but they were adjusted using a combination of parameter estimation and trial and error to produce a set of predicted pressures and well discharge that correlate best with observed values. The fracture is nearly flat-lying at a depth of 3.0 m, and it is nearly circular, so its geometry is similar to the axisymetric conditions of the model. The contact between the upper and lower layers in the model was assumed to be horizontal at a depth of 2.5 m. Fracture aperture distribution was calculated using Murdoch (2002; Eqs. (7) and (8)) with a sand volume of 0.3 m^3 and a depth of 3.0 m. Pressure at the well was set to 97.3 kPa based on field observations. The model typically converged in 1500 to 2000 iterations with a tolerance of 5.0×10^{-6}.

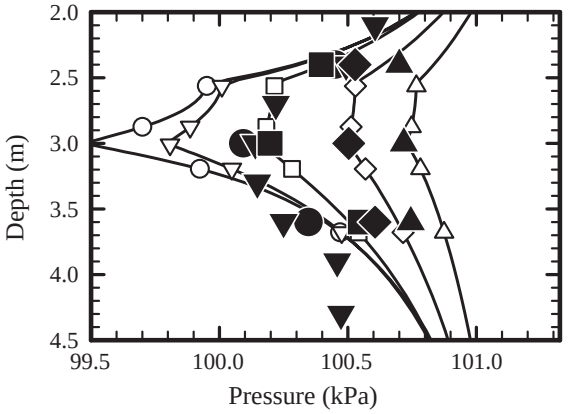

Fig. 7. Gas pressure as a function of depth and radial distance determined theoretically (lines and open symbols) and observed at piezometers (filled symbols). Radial distance=0.3 m (circle), 0.6 m (inverted triangle), 1.5 m (square), 3.0 m (diamond), 4.5 m (triangle).

The pressures predicted by the numerical model fit the observed pressures from field experiments with a correlation coefficient of $r=0.87$ (Fig. 7). The model predicts a discharge 0.0138 m^3/s (28.9 scfm), which is similar to observations in the field of 0.0133 m^3/s (28.0 scfm). Pressures predicted by the model are overestimated in close proximity to the fracture, with a maximum difference of 0.6 kPa (0.006 atm) occurring closest to the extraction well at the depth of the fracture (Fig. 7).

Minimizing the residuals between predicted and observed pressure and flow data estimates permeabilities of the upper layer of $k_h=0.12\times10^{-11}$ m^2 and $k_v=0.0085\times10^{-11}$ m^2, and permeabilities of the lower layer of $k_h=1.32\times10^{-11}$ m^2 and $k_v=0.44\times10^{-11}$ m^2. Those vertical permeabilities are remarkably similar to values obtained from Shelby tube samples (Table 1). The permeability of the fracture was estimated to be 8.0×10^{-9} m^2, which is greater than lab measurements for the sand filling the fracture.

5. Discussion

Theoretical analyses and field observations presented above suggest that wellbore skin can markedly decrease, and hydraulic fractures can markedly increase the flow efficiency of SVE wells.

5.1. Well skin

Specific gas capacities were remarkably variable in view of the small areas containing the wells. They varied by a factor of 16 within 2 m^2 at the north site and by a factor of 6 within 3 m^2 at the south site. The variability is erratically distributed among the cluster. It is possible that the wells intersected erratically shaped

heterogeneities, but this would not account for the uniformly low flow efficiencies, particularly at the north site.

Skins on SVE wells probably can result from many factors, depending on the drilling method and the formation. Skins in water and oil wells commonly result from smearing of clay or penetration of drilling mud into the walls of the formation (Driscoll, 1986), and those processes could also cause skins to form around SVE wells. Many SVE wells are drilled with hollow-stem augers where the radius of the cutting bit is larger than that of the auger flights. Such a drilling system can deposit a layer of material on the wall of the borehole whose thickness is equal to the difference in diameter between the bit and the auger flights. This layer can be clay-rich and can have relatively low permeability where clays are interbedded in the subsurface, according to observations we made on excavated wells.

The smallest S_c values obtained during this study occurred at wells drilled with a machine auger, and slightly greater values occurred at wells where the screen section was adjacent to a hole made with a Shelby tube sampler. The largest S_c values occurred in holes made with a hand auger (Table 2). A similar relation between S_c and drilling method occurred at the south site, although the Shelby tube method was not used at the south site.

The radial dimension of the bit on the machine auger we used is approximately 1 cm larger than that of the auger flights. As a result, the annular space created by the drilling process is filled with material, and we suspect that the permeability of this material is less than that of the enveloping formation. Skin factors for the wells drilled with the machine auger are roughly 25. This value of skin factor could be produced by a skin 1 cm thick whose permeability is 0.007 k, or approximately 7×10^{-14} m^2. This permeability is typical of silt, according to Freeze and Cherry (1979; Table 2.2), which is common at the field site.

It seems likely that a skin reduced the specific gas capacity of the machine auger wells. Machine augering is probably the most common method for creating wells used for SVE, so it is of particular significance that this drilling method apparently produced a skin that caused a flow efficiency of 0.03 to 0.04 on four different wells at the north site, and 0.27 at one well at the south site. This means that the specific capacities of wells drilled using a machine auger were a few percent to roughly one quarter of what they should be for an ideal conventional well with no skin.

Hand augering produced wells with higher flow efficiencies than those bored with a machine auger. Flow efficiencies of three hand augered wells at the north site were in the range of 0.44 to 0.54, although one well was less, 0.035, a value more typical of machine augers. Flow efficiencies at the south site varied from 0.25 to 1.5. We expect that hand augering followed by brushing produced a bore with a relatively small amount of skin. It is noteworthy, however, that the specific gas capacity of most of the hand augered wells was less than half of that expected for an ideal well. The origin of a skin during hand augering is unclear; however, a flow efficiency of 0.5 can be produced by a remarkably thin skin (Fig. 4), and it seems feasible that even a hand auger could slightly smear or disrupt pores in saprolite.

An increase in water content in the vicinity of an SVE well can also significantly reduce gas phase permeability. Water contents could increase as a result of either the drilling or

completion process. Sealing the screened portion of the well with either hydrated bentonite or cement during completion could increase the water content and decrease the gas-phase permeability of the well. This effect would be particularly severe where fine-grained materials inhibited gravity drainage from the vicinity of wells. We were careful to use methods that would avoid placing water into the gravel pack. However, it was difficult to measure the water content adjacent to the gravel pack, so it is possible that the soil was moistened despite our precautions.

Turbulent flow in the vicinity of a screen is known to decrease the specific capacities of water wells (Bear, 1979), and it should also affect SVE wells. The effects of turbulent flow were absent from step-rate tests conducted over the range of flows we could create with available equipment. As a result, we ignored the effect of turbulence, but it could be important in SVE wells under other circumstances.

Negative skin factors were observed at two conventional wells created with a hand-auger at the south site (Table 2). The reasons for this behavior are unclear. It is possible that heterogeneities, such as vertical fractures or pods of coarse-grained quartz and mica from relic pegmatite, increased the S_c of these wells.

5.2. Hydraulic fractures

The effectiveness of a hydraulic fracture on SVE discharge depends strongly on the contrast between the permeability of the material filling the fracture and that of the formation. A contrast in gas-phase permeability of roughly 50 appears to be required to increase flow efficiency by a factor of 2 for the dimensions of fractures considered here. This has practical ramifications because the gas-phase permeability of the coarsest sand used routinely for hydraulic fracturing at shallow depths is approximately 6×10^{-10} m^2. This places an upper limit approximately 10^{-11} m^2 for a formation where hydraulic fractures can cause significant improvement in specific gas capacity, assuming the fractures behave ideally and conventional wells with negligible skin can be created.

Wells intersecting hydraulic fractures commonly are evaluated by comparing their recovery rate to that of one or more conventional wells at the site (Schuring, 2002; Murdoch et al., 1994). The ratio of these values differs from the flow efficiency because specific capacities of conventional wells are probably less than the optimal value, S_{co}, used to estimate flow efficiency. Nevertheless, this approach has practical value (assuming the recovery rates are taken at the same pressure so that specific capacities are compared) because it provides an estimate of how much a fracture will change the specific capacity compared to the performance of wells that actually can be created at the site. As a result, the *effective flow efficiency*, $F_e = S_c/S_{control}$, for the fractured wells will exceed values of F calculated using Eq. (8) because well skin, or other effects, will typically reduce the S_c of conventional wells used for control.

Calculating the effective flow efficiencies for the wells intersecting hydraulic fractures is ambiguous because S_c for conventional vertical wells ranges over more than an order of magnitude. As a result, F_e depends on what value of specific capacity is used for the control well. One approach is to take mean values of S_c for $S_{control}$, and this gives a range of F_e from 17 to 51 at the north site, and 4 to 8 at the south site,

depending on whether the arithmetic or geometric means are used. However, F_e could be as high as 133 if only data from the fours wells created with a machine auger at the north site are used to define $S_{control}$. Our initial intent was to only use wells bored with a machine auger for control because we reasoned that most SVE wells probably were created using this drilling method. This would have increased the performance of wells intersecting fractures because other methods, like hand augering, could produce wells with considerably greater S_c. However, hand augering is impractical for many SVE applications.

Not all fractures created to improve well performance are filled with sand. Cracks created by rapidly injecting air into a well (pneumatic fractures), or those made by explosives are typically held open by asperities on their surfaces (Schuring, 2002). Cracks held open by asperities are commonly evaluated by their equivalent aperture (Tsang, 1992; Novakowski, 1988), rather than the thickness and permeability of material filling them. One method for estimating equivalent aperture of a crack representing a sand-filled hydraulic fracture is (Murdoch et al., 1994; Tsang, 1992)

$$\delta_e = (12 k_{frx} \delta)^{1/3} \tag{10}$$

It follows that the equivalent aperture of a crack representing the baseline hydraulic fracture used in this work ($\delta = 0.005$ m, $k_{frx} = 2 \times 10^{-10}$ m^2) is 230 microns. Cracks with similar apertures have been measured in dolomite by Novakowski (1988). The results presented in Figs. 5 and 6 can be generalized to cracks held open by asperities by relating equivalent aperture to k_{frx} and δ using Eq. (10).

6. Conclusions

The basic performance of a well used for soil vapor extraction can be described using specific gas capacity, S_c, which relates the volumetric air discharge rate at standard pressure to the applied suction at the well. A modest wellbore skin whose thickness is a few millimeters and gas phase permeability is 0.01 of the enveloping formation can reduce S_c by a factor of 2 or more (Fig. 4). Even a more permeable skin whose permeability is 0.1 k and thickness is 1 cm can significantly reduce S_c. Field data from tests in silty saprolite show that the flow efficiency of conventional SVE wells created with a machine auger is less than 0.1, and this can be explained if the well screen is enveloped by a skin 1-cm thick with a gas-phase permeability of 0.007 k (Fig. 4).

Flat-lying hydraulic fractures filled with sand will increase the S_c of SVE wells by amounts that depend on the size of the fracture and ratio between k_{frx} and k (Figs. 5 and 6). A minimum ratio (k_{frx}/k) of 50 is required to increase S_c by at least a factor of 2 (Fig. 5). The permeability of the coarse-grained sand used in this work is 6×10^{-10} m^2, so the upper limit of k that can be expected to significantly benefit from hydraulic fracturing is approximately 10^{-11} m^2.

Flow efficiencies between 10 and 50 are predicted for k_{frx}/k in the range of 10^3 to 10^4 (Fig. 5). This range of k_{frx}/k could be achieved by filling hydraulic fractures in silty clay

with coarse-grained sand, for example. Flow efficiencies of wells intersecting hydraulic fractures in saprolite were calculated to be between 3 and 5, whereas theoretical analyses predict values of F of approximately 3. Theoretical analyses are able to predict the distribution of pressure in the vicinity of a hydraulic fracture intersecting a well with reasonable accuracy (Fig. 7). The largest error occurs in the vicinity of the well, where the analysis overestimates the observed pressures.

Effective flow efficiencies for wells intersecting hydraulic or pneumatic fractures (Schuring, 2002; Murdoch et al., 1994) are commonly in the range of 10 to 50, but they rarely exceed 50. Similar values were obtained during this study. Effective flow efficiencies are determined by comparing the specific capacity of a well intersecting a hydraulic fracture to an actual conventional well at the site. Effective values exceeded theoretical flow efficiencies during this study because the conventional wells were damaged by skin.

Acknowledgements

We appreciate support from the National Science Foundation under grant EAR 9876124. Any opinions, findings, conclusions, or recommendations expressed in this material are those of the authors and do not necessarily reflect the views of the National Science Foundation. We thank John Gierke for his helpful review, along with those of an anonymous reviewer and the associate editor. Discussions with Ron Falta and the assistance of Rich Hall are also appreciated.

Appendix A

Integrating the solution for point source over a distance L along the z axis in an infinite, anisotropic media gives

$$f(L,\hat{r},z) = C_1 \ln\left(\frac{L-2z+\sqrt{4\hat{r}^2+(L-2z)^2}}{-(L+2z)+\sqrt{4\hat{r}^2+(L+2z)^2}}\right) \tag{A1}$$

$$\hat{r} = \left(\sqrt{\frac{k_z}{k_r}}\right) r \tag{A2}$$

A series is used to satisfy the upper and lower boundary conditions (Eqs. (2a)–(2e)), giving

$$\begin{aligned}\lambda(r,z,k_r,k_z,d,b,L) = {} & f(L,r,z+d) - f(L,r,z-d) \\ & + \sum_{n=1}^{\infty} -1^n \left(f(L,r,z+2nb-d) - f(L,r,z+2nb+d)\right. \\ & \left. + f(L,r,z-2nb+d) - f(L,r,z-2nb-d)\right)\end{aligned} \tag{A3}$$

The stream function for a line source in an infinite region is

$$g(r,z) = C_1\left(\sqrt{\hat{r}^2 + \left(z - \frac{L}{2}\right)^2} - \sqrt{\hat{r}^2 + \left(z + \frac{L}{2}\right)^2}\right) \tag{A4}$$

and the upper and lower boundary conditions are obtained using the same series as Eq. (A3).

References

Amir, G., Abdul, A.S., 1993. Numerical investigations of optimal well spacing and the effect of screen length and surface sealing on gas flow toward an extraction well. J. Contam. Hydrol. 12 (1–2), 171–191.

Arps, J.J., 1955. How well completion damage can be determined graphically. World Oil: Production Section, April, 1955, pp. 225–232.

Baehr, A.L., Hult, M.F., 1991. Evaluation of unsaturated zone air permeability through pneumatic tests. Water Resour. Res. 27 (10), 2605–2617.

Bear, J., 1979. Hydraulics of Groundwater. McGraw Hill Book Company, New York. 569 pp.

Bradner, G.C., 2002. Effects of shallow induced fractures on the performance of soil vapor extraction wells. M.S. Thesis. Clemson University. 143 pp.

Brusseau, M., 1991. Transport of organic chemicals by gas advection in structured or heterogeneous porous media: development of a model and application to column experiments. Water Resour. Res. 27 (12), 318–3199.

Chen, X.H., 1997. Evaluation of two methods for determining soil gas permeabilities from pneumatic tests. Environ. Geosci. 4 (2), 58–67.

Driscoll, F.G., 1986. Groundwater and Wells. Johnson Filtration Systems, St. Paul Minn. 1089 pp.

Earlougher Jr., R.C., 1977. Advances in Well Testing. American Institute of Mining. pp. 8–10, 42–44.

Edwards, K.B., Jones, L.C., 1994. Air permeability from pneumatic tests in oxidized till. J. Environ. Eng. 120 (2).

Falta, R.W., Pruess, K., Chesnut, D.A., 1993. Modeling advective contaminant transport during soil vapor extraction. Ground Water 31 (6), 1011–1020.

Fetter, C.W., 2001. Applied Hydrogeology. Prentice Hall. 598 pp.

Fischer, U., Hinz, C., Schulin, R., Stauffer, F., 1998. Assessment of nonequilibrium in gas–water mass transfer during advective gas-phase transport in soils. J. Contam. Hydrol. 33 (1–2), 133–148.

Frank, U., Barkley, N., 1994. Remediation of low permeability subsurface formations by fracturing enhancement of soil vapor extraction. J. Hazard. Mater. 40, 191–201.

Freeze, R.A., Cherry, J.A., 1979. Groundwater. Prentice Hall, Englewood Cliffs, NJ.

Gierke, J.S., 2000. Remediation technologies: conventional vapor extraction. In: Looney, B.B., Falta, R.W. (Eds.), Vadose Zone Science and Technologies, vol. 2. Batelle Press, pp. 951–969.

Gierke, John S., Hutzler, N.J., McKenzie, D.B., 1990. Experimental and model studies of the mechanisms influencing vapor extraction performance. Ground Water Manage. 4, 325–338.

James, A.L., 1994. Optimization of soil vapor extraction well design. M.S. Thesis, Clemson Universit. 131 pp.

Johnson, P.C., Kemblowski, M.W., Colthart, J.D., 1990. Quantitative analysis for the cleanup of hydrocarbon-contaminated soils by in-situ soil venting. Groundwater 28 (3), 413–429.

Jones, I., Lerner, D.N., Baines, O.P., 1999. Multiport Sock Samplers; a low cost technology for effective multilevel ground water sampling. Ground Water Monit. Remediat., 134–142 (Winter).

Kaleris, V., 2002. Influence of rate-limited sorption on the cleanup of layered soils by vapor extraction. J. Contam. Hydrol. 55 (1–2), 1–27.

Katyal, A.K., Parker, J.C., 1993. Optimizing the design of soil vacuum extraction systems. Ground Water Manage. 17, 273–284.

Klinkenberg, L.J., 1941. The permeability of porous media to liquids and gases. API Drilling and Production Practice, pp. 200–212.

Leach, B., Kosar, K., Ingraham, P.C., 1994. Pneumatic and hydraulic fracturing for enhanced in situ remediation of contaminated fine grained soils. Proceedings of the 1994 Focus Conference on Eastern Regional Ground Water Issues, pp. 537–549.

Liskowitz, J., Schuring, J., Mack, J., 1994. Application of pneumatic fracturing extraction for the effective removal of volatile organic compounds in low permeable formations. Focus Conference on Eastern Groundwater Issues, pp. 1–7.

Mohr, D.H., Merz, P.H., 1995. Application of a 2D air flow model to soil vapor extraction and bioventing case studies. Ground Water 33 (3), 433–444.

Murdoch, L.C., 1995. Forms of hydraulic fractures created during a field test in fine-grained glacial drift. Q. J. Eng. Geol. 28, 23–35.

Murdoch, L.C., 2000. Remediation of organic chemicals in the vadose zone. In: Falta, R., Looney, B. (Eds.), Vadose Zone, Science and Technology Solutions. Battelle Press, pp. 948–1247. Chapter 7.

Murdoch, L.C., 2002. Analysis of an idealized shallow hydraulic fracture. J. Geotech. Geoenviron. Eng., 1–36.

Murdoch, L.C., Slack, W., 2002. Forms of hydraulic fractures in shallow fine-grained formations. J. Geotech. Geoenviron. Eng., 1–44.

Murdoch, L.C., Wilson, D., Savage, K., Slack, W., Uber, J., 1994. Alternative Methods for Fluid Delivery and Recovery. USEPA/625/R-94/003.

Nelson, A.E., Horton, J.W., Clarke, J.W., 1990. Geologic Map of the Greenville 1°×2° Quadrangle, South Carolina, Georgia, and North Carolina. United States Geological Survey, pp. 1–3.

Novakowski, K.S., 1988. Comparison of fracture aperture widths determined from hydraulic measurements and tracer experiments. In: Hitchon, B., Bachu, S. (Eds.), Proceedings of the Fourth Canadian/American Conference on Hydrogeology. National Water Well Assoc., Dublin, OH, pp. 68–80.

Olson, M.S., Tillman, F.D., Choi, J.-W., Smith, J.A., 2001. Comparison of three techniques to measure unsaturated zone air permeability at Pictinny Arsenal, NJ. J. Contam. Hydrol. 53, 1–19.

Parker, J.C., Islam, M., 1997. Cost effectiveness of selected remediation technologies and design protocols. Bioremediation 4 (4), 341–346.

Pederson, T.A., Fan, C., 1992. Soil vapor extraction technology development status and trends. Proceedings of the Symposium on Soil Venting. United States Environmental Protection Agency, pp. 1–7.

Pollock, D.W., 1988. Semianalytical computation of paths lines for finite-difference models. Ground Water 26 (6), 743–750.

Rathfelder, K.M., Lang, J.R., Abriola, L.M., 1996. Mathematical modeling of rate-limited transport and biotransformation in the vadose zone. In: Aldama, A.A., Aparicio, J., Brebbia, C.A., Gray, W.G., Herrera, I., Pinder, G.F. (Eds.), Computational Methods in Subsurface Flow and Transport Problems. Proceedings of the International Conference on Computational Methods in Water Resources. 11, vol. 1, pp. 135–144.

Richardson, J.R., 2003. Forms of hydraulic fractures at shallow depths in Piedmont Soils. M.S. Thesis. Clemson University. 163 p.

Sacks, R.L., Dougherty, E.D., Guarnaccia, J.F., 1994. The design of optimal soil vapor extraction remediation systems using stimulated annealing. 1994 Groundwater Modeling Conference, pp. 343–350. United States, Fort Collins, CO, August 10–12.

Sawyer, C.S., Kamakoti, M., 1998. Optimal flow rates and well locations for soil vapor extraction design. J. Contam. Hydrol. 32 (1–2), 63–76.

Schulenberg, J.W., Reeves, H.W., 2002. Axi-symmetric simulation of soil vapor extraction influenced by soil fracturing. J. Contam. Hydrol. 57, 189–222.

Schuring, J.R., 2002. Fracturing Technologies to Enhance Remediation. Groundwater Remediation Technologies Analysis Center, Pittsburgh, PA. 58 pp.

Schuring, J.R., Jurka, V., Chan, P.C., 1991. Pneumatic fracturing to remove VOCs. Remediation, 51–67 (Winter).

Shan, C., Falta, R.W., Javandel, I., 1992. Analytical solutions for steady-state gas flow to a soil vapor extraction well. Water Resour. Res. 28 (4), 1105–1120.

Sowers, G.F., Richardson, T.L., 1983. Residual soils of the Piedmont and Blue Ridge. Transportation Research Record, vol. 919. National Academy Press, Washington, DC, pp. 10–20.

Streltsova, T.D. 1988. Well Testing in Heterogeneous Formations. John Wiley and Sons. P. 21, 158–160.

Sun, Y.H., Yeh, W.W.G., 1998. Location and schedule optimization of soil vapor extraction system design. J. Water Resour. Plan. Manage. 124 (1), 47–58.

Sun, Y.H., Davert, M.W., Yeh, W.W.G., 1996. Soil vapor extraction system design by combinatorial optimization. Water Resour. Res. 32 (6), 1863–1873.

Tsang, Y.W., 1992. Usage of "equivalent apertures" for rock fractures derived from hydraulic and tracer tests. Water Resour. Res. 28 (5:1), 451–455.

USEPA, 1991. Soil Vapor Extraction Technology Reference Handbook. EPA/540/2/91/001.

Van Everdingen, A.F., 1953. The skin effect and its influence on the productive capacity of a well. Petrol. Trans. 198, 171–176.

Wang, H.F., Anderson, W.P., 1982. Introduction to Groundwater Modeling: Finite Difference and Finite Element Methods. Academic Press, pp. 26–28.

Wolf, A., Murdoch, L.C., 1993. A field test of the effect of sand-filled hydraulic fractures on air flow in silty clay till. As Appears in the Proceedings from the Seventh National Outdoor Action Conference.

Yoon, H., Kim, J.H., Liljestrand, H.M., Khim, J., 2002. Effect of water content on transient nonequilibrium NAPL-gas mass transfer during soil vapor extraction. J. Contam. Hydrol. 54 (1–2), 1–18.